Anti–CTLA-4 therapy requires an Fc domain for efficacy

Jessica R. Ingram[a], Olga S. Blomberg[b], Mohammad Rashidian[b], Lestat Ali[a], Scott Garforth[c], Elena Fedorov[c], Alexander A. Fedorov[c], Jeffrey B. Bonanno[c], Camille Le Gall[b], Stephanie Crowley[a], Camilo Espinosa[a], Tamara Biary[d], Edmund J. Keliher[e,f], Ralph Weissleder[e,f], Steven C. Almo[c], Stephanie K. Dougan[a], Hidde L. Ploegh[b,1], and Michael Dougan[d,1]

[a]Department of Cancer Immunology and Virology, Dana–Farber Cancer Institute, Boston, MA 02215; [b]Program in Cellular and Molecular Medicine, Children's Hospital Boston, Boston, MA 02115; [c]Department of Biochemistry, Albert Einstein College of Medicine, Bronx, NY 10461; [d]Division of Gastroenterology, Massachusetts General Hospital, Boston, MA 02114; [e]Center for Systems Biology, Massachusetts General Hospital, Boston, MA 02114; and [f]Department of Radiology, Massachusetts General Hospital, Boston, MA 02114

Contributed by Hidde L. Ploegh, March 5, 2018 (sent for review January 29, 2018; reviewed by John B. A. G. Haanen and Karl Dane Wittrup)

Ipilimumab, a monoclonal antibody that recognizes cytotoxic T lymphocyte antigen (CTLA)-4, was the first approved "checkpoint"-blocking anticancer therapy. In mouse tumor models, the response to antibodies against CTLA-4 depends entirely on expression of the Fcγ receptor (FcγR), which may facilitate antibody-dependent cellular phagocytosis, but the contribution of simple CTLA-4 blockade remains unknown. To understand the role of CTLA-4 blockade in the complete absence of Fc-dependent functions, we developed H11, a high-affinity alpaca heavy chain-only antibody fragment (VHH) against CTLA-4. The VHH H11 lacks an Fc portion, binds monovalently to CTLA-4, and inhibits interactions between CTLA-4 and its ligand by occluding the ligand-binding motif on CTLA-4 as shown crystallographically. We used H11 to visualize CTLA-4 expression in vivo using whole-animal immuno-PET, finding that surface-accessible CTLA-4 is largely confined to the tumor microenvironment. Despite this, H11-mediated CTLA-4 blockade has minimal effects on antitumor responses. Installation of the murine IgG2a constant region on H11 dramatically enhances its antitumor response. Coadministration of the monovalent H11 VHH blocks the efficacy of a full-sized therapeutic antibody. We were thus able to demonstrate that CTLA-4–binding antibodies require an Fc domain for antitumor effect.

immunotherapy | CTLA-4 | single-domain antibody | cancer | checkpoint blockade

Immunotherapy has become standard treatment for a range of human malignancies, showing outcomes that include long-term remissions (1–5). Ipilimumab, a monoclonal antibody that recognizes cytotoxic T lymphocyte antigen (CTLA)-4, was the first approved antitumor immunotherapy to target a regulatory "checkpoint" receptor (3, 5). However, ipilimumab is less effective and more narrow in the spectrum of tumors it targets compared with antibodies to the regulatory receptor programmed death (PD)-1 or its ligand PD-L1 (1–3, 6). Their mechanism of action includes (re)activation of cytotoxic T cells that recognize neoantigens, but the details that link antibody binding to downstream T cell-mediated antitumor responses are not completely understood, particularly for CTLA-4–targeted therapies (7, 8).

As others have noted, expression of CTLA-4 and other inhibitory receptors on tumor infiltrating lymphocytes, particularly CD8 T cells, correlates with response to immunotherapy in patients with melanoma, but monitoring these markers requires surgical intervention (6). Developing noninvasive mechanisms to track the interaction between the immune system and tumors, including the expression of regulatory receptors, is thus of potential clinical value. Immuno-PET offers exquisite sensitivity and specificity for targets that are accessible via the bloodstream. Several groups have used this technique in mice to track other immune cell markers, but monitoring of CTLA-4 expression has not been reported to our knowledge (9–11).

CTLA-4 is a member of the IgV domain superfamily, and serves as a coinhibitory receptor expressed on regulatory T cells (Tregs) and activated $CD4^+$ and $CD8^+$ T cells (12, 13). It competes with CD28 for binding to B7-1 (CD80) and B7-2 (CD86). CTLA-4 expression is associated with diminished T cell activation in vitro, although CTLA-4 does not deliver its own inhibitory signal and may instead function through disruption of the B7–CD28 axis (12, 13). CTLA-4 is predominantly sequestered in the endosomes of resting cells, and aggregates at the cell membrane during T cell receptor engagement, with recycling from the cell surface (14). CTLA-4 deficiency in mice—or haploinsufficiency in humans—is associated with severe autoimmune disease; treatment with anti–CTLA-4 antibodies induces many of these same manifestations in patients (15–19). In murine models, specific loss of CTLA-4 in the Treg lineage phenocopies CTLA-4 deficiency, and is associated with decreased peripheral Tregs function (20). However, induced loss of CTLA-4 in adult animals does not cause overt autoimmunity (21).

Mouse models of antitumor immunity predicted the therapeutic potential of anti–CTLA-4 monoclonal antibody therapy (22). In the B16 melanoma model, anti–CTLA-4 antibodies can cure most mice when used in combination with an antitumor vaccine (22, 23). The response to this treatment depends entirely

Significance

Ipilimumab, an antibody that recognizes cytotoxic T lymphocyte antigen (CTLA)-4, was the first approved "checkpoint"-blocking anticancer therapy. In mice, the response to antibodies against CTLA-4 depends entirely on expression of the Fcγ receptor. We developed H11, an alpaca heavy chain-only antibody fragment against CTLA-4 that lacks an Fc portion and inhibits interactions between CTLA-4 and its ligand. By using H11 to visualize CTLA-4 expression in the whole animal, we found that accessible CTLA-4 is largely confined to the tumor; however, H11 treatment has minimal effects on antitumor responses. Installing the murine IgG2a constant region on H11 greatly enhances antitumor response. We were thus able to dissociate CTLA-4 blockade from CTLA-4–dependent receptor engagement as an explanation for the antitumor effect.

Author contributions: J.R.I., R.W., S.C.A., S.K.D., H.L.P., and M.D. designed research; J.R.I., O.S.B., M.R., L.A., S.G., E.F., A.A.F., J.B.B., C.L.G., S.C., C.E., T.B., E.J.K., S.K.D., and M.D. performed research; J.R.I., O.S.B., M.R., L.A., S.G., E.F., A.A.F., J.B.B., C.L.G., S.C., C.E., T.B., E.J.K., R.W., S.C.A., S.K.D., H.L.P., and M.D. analyzed data; and J.R.I., H.L.P., and M.D. wrote the paper.

Reviewers: J.B.A.G.H., Netherlands Cancer Institute; and K.D.W., Massachusetts Institute of Technology.

The authors declare no conflict of interest.

Data deposition: The atomic coordinates and structure factors have been deposited in the Protein Data Bank, www.wwpdb.org (PDB ID code 5ESM).

[1]To whom correspondence may be addressed. Email: hidde.ploegh@childrens.harvard.edu or mldougan@partners.org.

This article contains supporting information online at www.pnas.org/lookup/suppl/doi:10.1073/pnas.1801524115/-/DCSupplemental.

Published online March 26, 2018.

on expression of the Fcγ receptor (FcγR), which may facilitate antibody-dependent cellular phagocytosis by tumor-associated macrophages (23, 24). A decrease in intratumoral Tregs correlates positively with therapeutic efficacy in B16 melanoma, with FcγRIV$^{-/-}$ mice showing tumor outgrowth and maintenance of intratumoral Tregs after CTLA-4 antibody treatment (23). In mouse models of colon cancer, exchange of the anti–CTLA-4 antibody to the IgG1 Fc domain or to an IgG1 variant mutated to prevent FcγR-binding abrogates the antitumor effect (25).

The precise role of CTLA-4 blockade in the therapeutic effect of CTLA-4–binding antibodies nonetheless remains unclear. FcγR-deficient mice may differ from WT animals in other critical aspects of the antitumor response, which may be particularly relevant in the setting of the vaccination models used. Alterations in FcγR binding may also affect tissue penetration or retention of CTLA-4 antibodies, and account for changes in therapeutic efficacy. There is no obvious explanation why intratumoral Tregs would be preferentially targeted by anti–CTLA-4 antibodies while leaving peripheral Tregs intact. Such tissue specificity is not seen for other depleting antibodies. Higher expression of CTLA-4 on tumor-associated Tregs and increased numbers of FcγRIV-positive tumor-associated macrophages have both been proposed as mechanisms underlying the tumor specificity of Treg depletion, although neither mechanism can be considered rigorously established (23–25). Clarifying this issue in a mouse model may help determine whether similar mechanisms apply to ipilimumab-treated patients.

To address this, we developed H11, a high-affinity alpaca heavy chain-only antibody fragment (VHH) against CTLA-4 (26).The H11 VHH lacks an Fc portion, binds monovalently to CTLA-4, and is more potent than a full-sized anti-mouse CTLA-4 monoclonal antibody at blocking CTLA-4 interactions with its ligand. We show the mechanism of this blocking activity at atomic resolution. By imaging live mice, we find that a radiolabeled form of H11 localizes specifically to the tumor. Even so, CTLA-4 blockade by H11 has minimal effects on antitumor responses. Conjugation of the anti–CTLA-4 VHH to the murine IgG2a constant region dramatically enhances the antitumor response, and coadministration of H11 as a monomer blocks the efficacy of a full-sized antibody. We were thus able to show that simple CTLA-4 blockade was insufficient to induce substantial antitumor effects in the absence of Fc-dependent activity.

Results

Generation of the αCTLA-4 VHH H11. To generate a VHH against CTLA-4, we immunized an alpaca with recombinant mouse CTLA-4 extracellular domain (ECD) fused to an Fc domain, and constructed a phage display library from the immunized animal following previously described methods (Fig. S1*A*) (10, 27). Panning of the library against recombinant mCTLA-4 ECD-Fc identified a clone termed H11, which bound CTLA-4 with high affinity. H11 was expressed in high yield as a soluble protein in *Escherichia coli* (Fig. S1 *B–D*). Specificity of H11 for recombinant mouse CTLA-4 was determined by immunoblot (Fig. 1*A*) and in a plate-binding assay, showing binding with a K_d in the low nanomolar range (Fig. 1*B*). H11 did not recognize several other Fc fusion proteins, such as other IgV domain-containing immune receptors including B7-1 and CD28, nor did it recognize human CTLA-4 ECD (Fig. 1*C* and Fig. S1 *E* and *F*) (13). H11 bound to CTLA-4 in permeabilized spleen cells, showing preferential staining of CD3$^+$CD4$^+$CD25$^+$ T cells, as has been reported for conventional anti–CTLA-4 antibodies (20, 21). This staining was specific for CTLA-4, as H11 did not bind to cells from animals in which CTLA-4 had been conditionally deleted (Fig. 1*D*) (21).

H11 Blocks CTLA-4 Interactions with Its Ligands. To date, no structures of anti–CTLA-4 antibodies in complex with mouse CTLA-4 are available, although the crystal structure of ipilimumab bound to human CTLA-4 was recently reported (28). We crystallized and determined the structure of H11 in complex with the mCTLA-4 ECD at 2.18-Å resolution (Fig. 1*E* and Table S1).

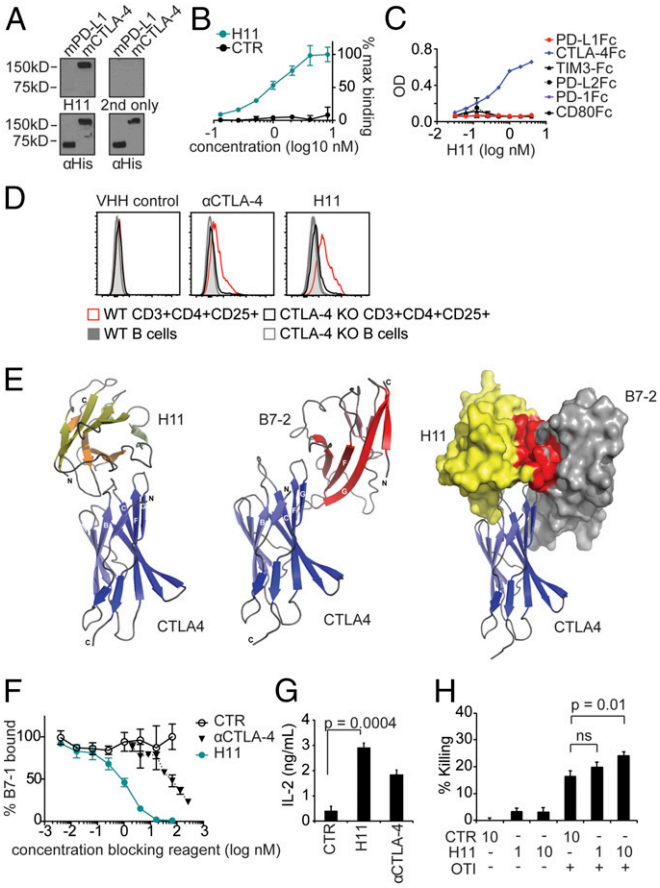

Fig. 1. H11 recognizes CTLA-4. (*A*, *Top*) H11 immunoblot against His-tagged murine PD-L1 (mPD-L1) and mCTLA-4. "2nd only" refers to staining with secondary antibody alone. (*A*, *Bottom*) Corresponding anti-His immunoblots as loading controls. (*B* and *C*) Biotinylated H11 or VHH control (CTR) were incubated with plate-bound mCTLA-4-Fc (*B*) or recombinant Fc fusion proteins as indicated (*C*). Binding was detected by using streptavidin-HRP and tetramethylbenzidine (TMB). Data are normalized to the maximum signal (*B*) or represented as OD. Error bars show SD. (*D*) Flow cytometry on splenic populations as indicated from WT and CTLA-4 (inducibly) deleted (KO) mice using H11 or αCTLA-4 antibody as indicated. (*E*, *Left*) Ribbon drawing of the CTLA-4:H11 complex (PDB ID code 5ESM). CTLA-4 is in blue; H11 is in yellow. (*E*, *Middle*) Overall structure of CTLA-4:B7-2 complex (PDB ID code 1I85). CTLA-4 is in blue; B7-2 is in red. (*E*, *Right*) Surface rendering of CTLA-4 binding partners highlighting the steric clash between H11 and B7-2 binding sites (residues from H11 within 4.5-Å distance of B7-2, and vice versa, are colored red). (*F*) B7-1-Fc was incubated with plate-bound CTLA-4-Fc in the presence of H11, αCTLA-4, or VHH control (CTR). Binding was detected by using a biotinylated polyclonal antibody against B7-1 and streptavidin-HRP developed with TMB. Error bars show SD. (*G*) CD4$^+$ T cells were isolated from the spleen by positive selection using magnetic beads and stimulated with plate-bound αCD3 and B7-1-Fc for 96 h in the presence of VHH or antibody as indicated. Secreted IL-2 levels were measured by ELISA. (*H*) Activated OT-I cells were cultured with IFN-γ–treated B16-ova cells in the presence of H11 or control VHH at the indicated concentrations. Cell viability was determined using CellTiterGlo and normalized to untreated cells. (*G* and *H*) Error bars show SEM. *A–D* and *F–H* represent at least three independent experiments. ns, nonsignificant.

H11 binds to a conformational epitope on the mCTLA-4 surface, near the ^{97}MYPPPY^{102} motif, which is essential for interaction with the B7-1 (CD80) and B7-2 (CD86) ligands (Fig. 1*E*) (13, 28). Comparison of corresponding mouse CTLA-4 residues in Protein Data Bank (PDB) entries 5E5M and 5E56 reveals substantial rearrangement of the CTLA-4 BC loop (residues Ser24 to Glu31) to accommodate insertion of the H11 loop (residues Thr100 to Thr103). In particular, CTLA-4 Thr29 rotates toward the hydrophobic core, whereas Asp30 flips outward

to form a hydrogen bond with H11 Tyr39. Large shifts are also observed for CTLA-4 His27 (~6 Å) and Asn28 (~8.5 Å), which form polar interactions with H11 Ala35 backbone NH and Lys99 side-chain NZ, respectively. Additionally, the CTLA-4 C′C″ loop (Thr53 to Thr57) is displaced as a rigid body by ~1.5 Å, whereas the DE loop remains almost completely unchanged. Collectively, these shifts create a pocket suitable for binding of H11 Gly101 and Leu102. The H11 strand containing Ser33 to Tyr39 is positioned above the CTLA-4 BC loop, whereas the connected H11 strands containing Trp49 to Ser56 and Ser57 to Thr61 contact the proline-rich stretch (residues 99–101) and Phe103 on the B7 recognition surface of CTLA-4. Local structural alignment of the MYPPPY loops in the CTLA-4 complexes formed with H11, B7-1, and B7-2 reveals that residues involved in B7-ligand recognition do not exhibit appreciable reorganization upon H11 engagement.

H11 and the B7 ligands share overlapping binding sites on the CTLA-4 surface in the vicinity of the MYPPPY loop; H11 is therefore predicted to sterically interfere with association of the B7s with CTLA-4 (Fig. 1*E*). Calculations (29) estimate the overlap volume between H11 and B7-2, positioned on CTLA-4 in their respective binding poses, to be ~830 $Å^3$. We confirmed disruption of receptor-ligand binding by H11 in plate-binding assays with immobilized CTLA-4 and soluble B7-1-Fc. The inclusion of H11 prevented B7-1-Fc binding with ~100-fold greater potency than the commonly used anti-mouse CTLA-4 antibody 9H10 (Fig. 1*F*) (22). Consistent with its ability to disrupt CTLA-4 interactions with the B7s, H11 enhanced cytokine production from αCD3/B7-1 stimulated CD4 T cells in vitro (Fig. 1*G*) and modestly enhanced cytotoxicity of activated OT-I T cells against B16-ovalbumin (B16-ova) (Fig. 1*H*).

In Vivo Surface Expression of CTLA-4 Is Confined to the Tumor Microenvironment. To test whether H11 could bind CTLA-4 in vivo, we generated an H11 construct that contained a C-terminal LPETG sortase motif. This allowed the installation of ^{18}F or ^{89}Zr for immuno-PET in accordance with methods we have used to image a variety of immune receptors (9, 10, 30). Immuno-PET with ^{18}F-H11 showed no signal above background in WT mice (Fig. 2*A*), but showed weak staining of injected B16 tumors, likely through binding of activated T cells or Tregs in the tumor microenvironment (Fig. 2*B*). Staining of the organs of elimination is luminal and common to many VHH-based imaging reagents (10). The signal was further enhanced by conjugation of H11 to a 20-kD PEG moiety (H11-PEG20), which can substantially improve the signal-to-noise ratio in VHH-based immuno-PET (Fig. 2*C*) (11). Zr 89-labeled H11-PEG clearly delineated s.c.-injected B16 melanoma as well as an accompanying GM-CSF–secreting autologous irradiated tumor vaccine (GVAX; Fig. 2*C*) (31). Consistent with the high affinity of H11 for CTLA-4, these images were obtained despite the presence of circulating full-sized anti–CTLA-4 antibodies (9H10) used therapeutically in these animals and with the imaging reagent at a far lower dose, though we did not experimentally establish that the anti–CTLA-4 antibodies were saturating.

Mice imaged with H11-PEG showed no difference in overall survival compared with control animals imaged with an unrelated VHH (Fig. 2*D*). This shows the safety of using CTLA-4 imaging even in a setting in which CTLA-4 is targeted therapeutically. These images thus show the distribution of surface-expressed CTLA-4 in a naïve and in a live tumor-bearing host in a syngeneic setting (32). We find that CTLA-4 is accessible on the surface of target cells within the tumor microenvironment, but is otherwise largely inaccessible or present at levels undetectable by PET elsewhere in the body, including lymphatic tissue.

CTLA-4 Blockade Alone Does Not Promote Antitumor Responses. CTLA-4–blocking antibodies were first shown to have antitumor efficacy against B16 melanoma in a tumor vaccination model using GVAX (22). When delivered prophylactically, GVAX provides potent, tumor-specific immunity sufficient to prevent engraftment of live B16 cells (31). When used concurrently with a tumor challenge, GVAX initiates antitumor responses that fail to slow tumor growth, but that can dramatically enhance other immune therapies, including combination therapy with anti–CTLA-4 antibodies, to achieve a cure (22, 33–35). B16 GVAX is thus a preclinical model for the interaction between the immune system and melanoma in humans, in which endogenous immune responses are common, but often insufficient to control tumor growth in the absence of additional immunotherapy (1).

Despite its potency in vitro, the combination of H11 with GVAX had minimal efficacy in vivo compared with the full-sized anti–CTLA-4 antibody 9H10 (Fig. 3*A*). VHHs have a short circulatory $t_{1/2}$—although their tissue $t_{1/2}$ can be considerably longer—which may create a pharmacokinetic barrier that precludes effective treatment with H11 (9, 27). However, a failure to reach the tumor in adequate concentrations does not account for the observed lack of efficacy in vivo. Inducing possible cross-linking of CTLA-4 by dimerization [$(H11)_2$; Fig. S2 *A–E*] or extension of the $t_{1/2}$ through dimerization or the addition of a PEG moiety (H11PEG) had no appreciable effect on efficacy (Fig. 3 *A* and *B*). Moreover, administration of H11 strongly reduced therapeutic

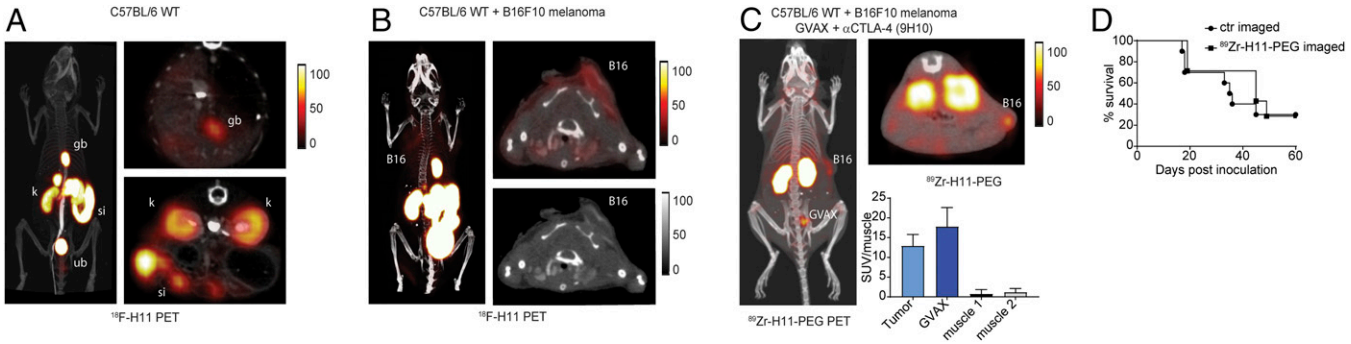

Fig. 2. In vivo imaging of CTLA-4 distribution by immuno-PET. PET-CT images of a naïve C57BL/6 WT mouse (*A*) or a mouse bearing a B16F10 melanoma (*B*) imaged with ^{18}F-H11. (*A* and *B*, *Left*) Three-dimensional projection images overlaying the PET signal and the corresponding CT. (*Upper Right*) Transverse PET-CT overlays. (*A*, *Bottom Right*) Transverse PET-CT overlay of the abdomen capturing the organs of elimination: kidney (kd), intestines (int), gallbladder (gb), and urinary bladder (bl). (*B*, *Lower Right*) Transverse CT only. (*A* and *B*) Images are all window-leveled to the same intensity. (*C*) C57BL/6 WT mouse inoculated with B16 melanoma and treated with a combination of a tumor vaccine (GVAX) and anti-CTLA-4 (clone 9H10). After 10 d of treatment, mice were imaged with ^{89}Zr-H11-PEG. The tumor (B16) and the vaccination site (GVAX) are marked. Three-dimensional projection image (*Left*) and transverse PET-CT overlays (*Top Right*) as in *A* and *B*. (*Bottom Right*) Standardized uptake values (SUVs) for ^{89}Zr-H11-PEG imaged mice for tumor, GVAX, and two different muscle sites normalized to the average muscle signal. (*D*) Survival curve for mice imaged with ^{89}Zr-H11-PEG compared with ^{89}Zr-VHH-PEG control (n = 10). Results represent at least two independent experiments.

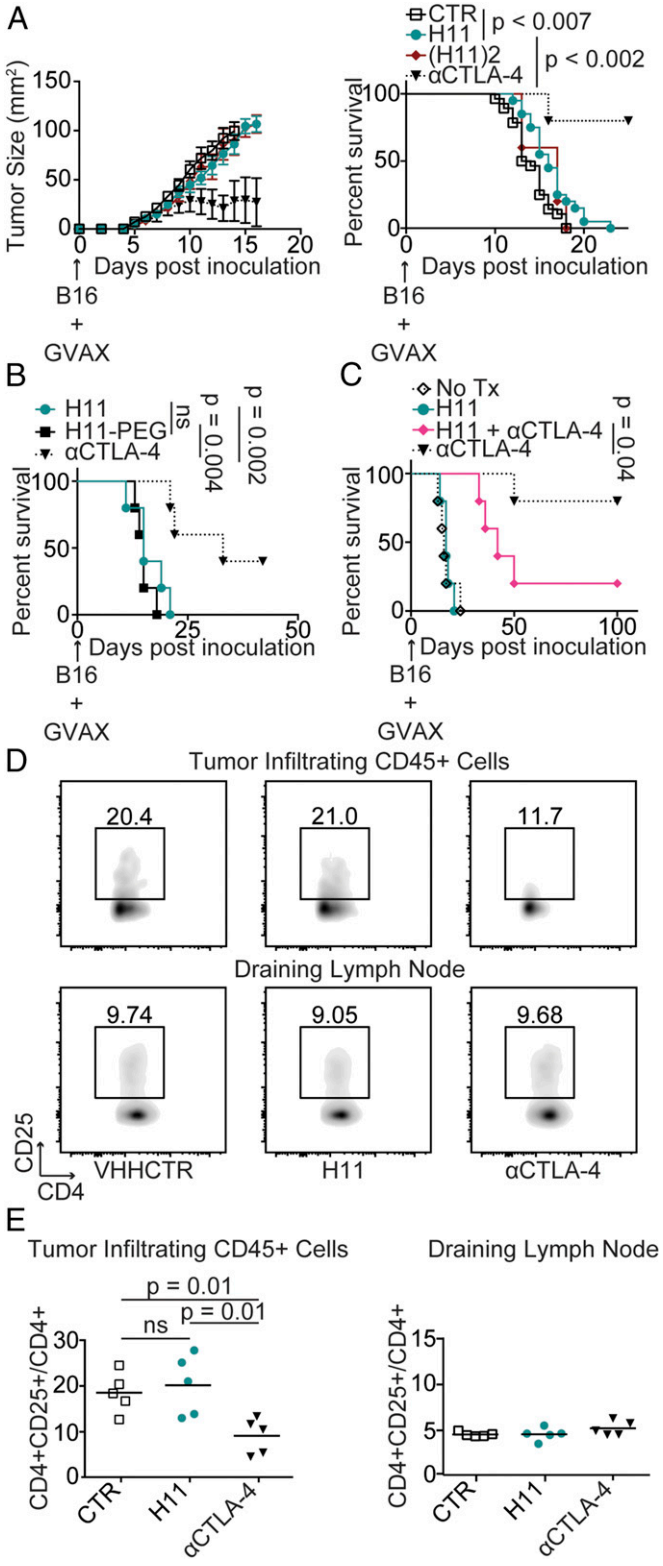

Fig. 3. H11 has minimal antitumor activity in vivo. (*A*) C57BL/6 mice were inoculated with 5×10^5 B16 cells and vaccinated with 5×10^5 GM-CSF–secreting B16 cells (GVAX) on day 0. Mice were treated daily with 200 μg VHH control (CTR), H11, or H11 dimer [$(H11)_2$] or every other day with 200 μg anti–CTLA-4 (αCTLA-4) antibodies, clone 9H10. (*Left*) Tumor size as measured by precision calipers. Error bars show SEM. Curves terminated when >50% of the group had been euthanized. (*Right*) Survival curve comparing treatment groups. Animals were euthanized when tumor reached 125 mm^2. Control ($n = 28$), H11 ($n = 20$), $H11_2$ ($n = 5$), αCTLA-4 ($n = 5$). (*B* and *C*) Survival curves for mice inoculated with B16 and vaccinated as in *A* on day 0. (*B*) Mice were treated with 200 μg H11 daily or three times weekly with H11PEG or αCTLA-4 given at equimolar doses. (*C*) Starting on day 1, mice were left untreated or were treated daily with 200 μg H11, three times weekly with 200 μg αCTLA-4, or with a combination of the two treatments. (*B* and *C*) $n = 5$ for all groups. Results represent at least two independent experiments. (*D* and *E*) Mice were inoculated with B16 and vaccinated as in *A* on day 0. Mice were treated daily with VHH control (CTR) or H11 or three times weekly with αCTLA-4 antibodies starting on day 1. On day 10, mice were euthanized and tumor-infiltrating leukocytes (TILs) were isolated from resected tumors, or lymphocytes were isolated from the draining lymph node and analyzed by flow cytometry using the indicated antibodies. (*D*) Flow cytometry plots. (*E*) Quantification of data from *D* including multiple animals. ns, nonsignificant.

efficacy of 9H10, showing that H11 can readily reach its site of action and compete with the full-sized antibody in vivo (Fig. 3*C*). The response to anti–CTLA-4 is correlated with a relative decrease in Tregs in the tumor microenvironment, a function linked to FcγR engagement (23–25, 36). Consequently, H11, which lacks an Fc domain, may be unable to induce the relative reduction in Tregs caused by full-sized antibodies that target CTLA-4. Indeed, intratumoral Tregs were not affected by treatment with H11, in contrast to treatment with the anti–CTLA-4 antibody 9H10 (Fig. 3 *D* and *E*). Blocking B7-1 engagement by CTLA-4 is thus of minor protective value, consistent with a primary role for Fc-dependent depletion of Tregs in the therapeutic response to anti–CTLA-4 in vivo (23–25, 36). Even highly potent CTLA-4 blockade is insufficient alone to achieve optimal antitumor effect.

High-Affinity H11–IgG2a Conjugate Enhances Antitumor Immunity. To test the hypothesis that FcγR engagement is an essential component of the efficacy of anti–CTLA-4–based therapy, we conjugated H11 to murine IgG2a through genetic fusion or through a sortase-mediated protein ligation (Fig. 4 *A* and *B* and Fig. S2 *F* and *G*) (37). We used mammalian cells to produce both Fc fusion conjugates, which retained their binding affinity for CTLA-4 in vitro (Fig. 4*C* and Figs. S2 *H*, *J*, and *K*). Treatment of B16 melanoma by coadministration of the genetic H11 IgG2a fusion (H11–IgG2a) and GVAX led to a relative reduction in Tregs in the tumor microenvironment, comparable to what was achieved by treatment with the monoclonal antibody 9H10 (Fig. 4 *D* and *E*). This relative reduction correlated with a trend toward increased T cells, with H11–IgG2a showing a significant relative expansion ($P < 0.03$) of CD4 T cells compared with the full-sized 9H10 antibody (Fig. 4 *F* and *G*). No changes in cellular composition were observed in the spleen or the draining lymph node (Fig. S3). In contrast to treatment with the H11 VHH, the H11–IgG2a construct outperformed the monoclonal antibody when administrated at the same molar concentration, showing comparably high overall survival but a more rapid response to treatment, with more animals being fully tumor-free at the end of the experiment (Fig. 4*H*). The H11 Fc IgG2a sortase-mediated fusion (H11–GGG–Fc), which has an altered hinge region, showed considerably weaker in vivo activity (Fig. S2*I*). The improved antitumor effects of H11–IgG2a may be the result of a combination of higher potency, as demonstrated by in vitro binding assays, and its smaller size (~70 kDa for the H11–IgG2a fusion, compared with ~150 kDa for 9H10), which should favor tissue penetration, although the differences may also be attributable to the specific Fc sequence, which was a fully murinized IgG2a compared with the Syrian Hamster IgG sequence of 9H10.

The crystal structure of H11 bound to CTLA-4 predicts that a critical binding contact is made through VHH framework regions. To test this structural prediction, we mutated a key framework contact on H11 to generate a low-affinity fusion construct. Mutant (m) H11–IgG2a demonstrated weak affinity for CTLA-4

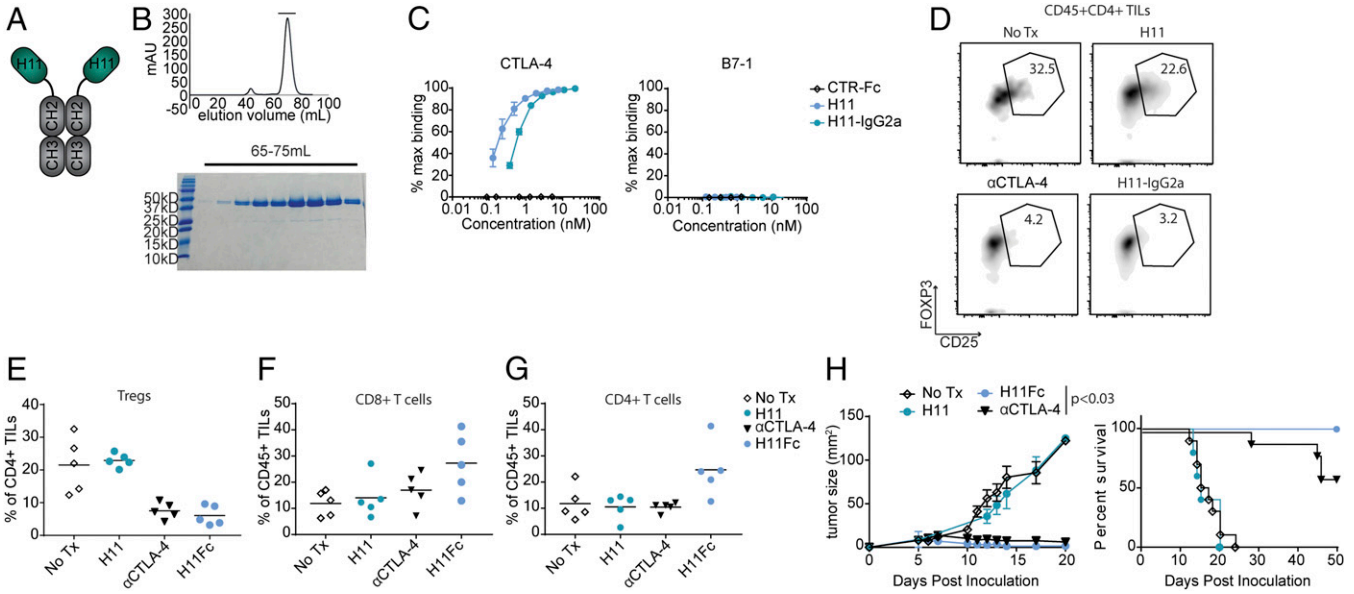

Fig. 4. H11 fusion to IgG2a restores therapeutic efficacy. (*A*) Schematic representation of H11–IgG2a. (*B*) H11–IgG2a size-exclusion chromatogram (*Top*) and Coomassie-stained SDS/PAGE (*Bottom*). (*C*) Biotinylated H11, H11–IgG2a, or VHH-Fc control (CTR-Fc) were incubated with plate-bound mCTLA-4-Fc (*Left*) or mB7-1-Fc (*Right*). Binding was detected and analyzed as in Fig. 1*B*. (*D–G*) Mice were inoculated with B16 and vaccinated as in Fig. 3*A* on day 0. Mice were treated daily with 100 μg H11 or twice weekly with 100 μg H11–IgG2a or 200 μg αCTLA-4 antibodies or were left untreated, starting on day 1. On day 11, mice were euthanized and TILs were isolated from resected tumors and analyzed by flow cytometry. (*D*) Flow-cytometry plots using the indicated antibodies. (*E*) Quantification of data from *D* including multiple animals. (*F* and *G*) Quantification of $CD8^+$ TILs (*F*) and $CD4^+$ TILs (*G*). (*H*) Mice were inoculated with B16, vaccinated, and treated as in *D–G*. (*Left*) Tumor growth curves; (*Right*) Overall survival (*$P < 0.05$). Results represent at least two independent experiments. Tx, treatment.

in vitro and substantially reduced antitumor efficacy in vivo, with all treated tumors ultimately progressing (Fig. S4).

Discussion

We generated a VHH that binds murine CTLA-4 with high affinity and blocks interactions between CTLA-4 and its ligand at lower concentrations than the widely used full-sized anti–CTLA-4 antibody 9H10. We crystallized the H11 VHH in complex with CTLA-4, providing a structural basis for its blocking activity in vitro. Despite its high affinity and CTLA-4–blocking properties in vitro, H11 VHH has minimal efficacy in vivo when administered as a monomeric antibody fragment. The short circulatory $t_{1/2}$ of VHHs poses a challenge to their therapeutic use (9, 27). Nonetheless, the lack of in vivo efficacy was clearly not the result of a failure to engage CTLA-4 in the tumor microenvironment. H11 VHH accumulates within the tumor, as seen by immuno-PET, yet we saw no enhanced antitumor activity by prolonging serum $t_{1/2}$ through PEGylation, or by dimerization of H11. The observation that VHH H11 outcompetes the monoclonal antibody in a therapeutic setting when coadministered with 9H10 and inhibits 9H10 activity is strong support for H11 efficiently reaching its in vivo target. This coadministration experiment demonstrates that blockade of CTLA-4, in the absence of FcγR engagement, has a dominant-negative effect.

Increasing evidence indicates a central role for FcγR in murine models. Responses to antibodies that target GITR or OX40 depend on their interactions with FcγRs, as does an IL-2–Fc fusion construct (24, 38). Modulation of FcγR interactions dramatically enhances the efficacy of anti-CD25 antibodies in vivo (39). In contrast, PD-1–blocking antibodies may be removed from their targets by FcγR binding, reducing efficacy (40). In several murine models of CTLA-4 blockade, Fc-FcγR interactions appear to be of central importance. Loss of FcγRIV renders CTLA-4 blockade inert in the B16F10 GVAX model, even though this finding does not exclude a necessary role for FcγRIV in the antitumor response that is not directly related to binding the therapeutic antibody. Exchange of the Fc domain on anti–CTLA-4 for one that has low affinity for FcγRs similarly diminishes the therapeutic activity of CTLA-4 blockade in two murine models of colon cancer (25). In neither mouse model was delivery of the altered antibodies to the tumor microenvironment assessed, opening up the possibility that FcγR-dependent antibody retention or trafficking into the tumor could contribute to, if not account for, the observed loss of activity. Our findings now support the conclusions of both of these earlier studies.

Whether the dominant role for FcγRs observed in mice is replicated in human patients treated with the analogous antibodies remains unclear (41). An increased CD8-to-Treg ratio has been associated with therapeutic responses in patients (35, 42), and the anti–CTLA-4 antibody ipilimumab can deplete human Tregs in vitro (35). Patients treated with ipilimumab do not definitively show Treg depletion, but this may relate to the difficulty of sampling adequately to draw an unambiguous conclusion (41, 43).

The efficacy of H11-based anti–CTLA-4 therapy is restored through its attachment to the Fc portion of murine IgG2a. This results in a modified chimeric antibody more potent in vivo than the conventional anti-mouse CTLA-4 antibody 9H10. Alteration of the FcγR-binding hinge region or the antigen-binding domain of the antibody strongly reduced therapeutic efficacy. These results support a model in which anti–CTLA-4 serves to decorate targeted cells with Fc domains, and that delivery of the Fc to the CTLA-4–expressing cell is responsible for therapeutic efficacy (23–25, 36). The most likely target in this model is the Treg, given its level of expression of CTLA-4, and the probability that binding to an Fc domain would lead to loss of the targeted cell, as we and others have observed in the microenvironment of treated tumors (23, 25).

We also provide high-resolution in vivo imaging of CTLA-4 distribution in a syngeneic setting by using immuno-PET and ^{18}F- and ^{89}Zr-functionalized versions of VHHs, as we have used successfully to image other immune receptors (11). Even though endogenous expression of CTLA-4 is low, its visualization by PET was helped by several properties of VHHs that yield improved resolution compared with full-sized antibodies. VHHs are small (~15 kDa) and readily penetrate tissue (26). With their short circulatory $t_{1/2}$, VHHs are rapidly cleared from the

circulation, improving the signal-to-background ratio (44). That H11-based imaging does not block 9H10's effect on survival is likely attributable to the small absolute amounts of H11 used for immuno-PET and the limited exposure in single time-point imaging. Given established methods to label VHHs for use in PET and the ready availability of PET imaging in the clinic, this method, if properly developed further for use in patients, may be useful to quantify intratumoral Tregs noninvasively (SI Discussion) (43).

Anti–CTLA-4 therapy in patients is associated with diverse, severe inflammatory toxicities, including a life-threatening colitis in a substantial fraction of patients (2, 4, 5, 19). At present, these toxicities are treated with broad immunosuppression, which nearly always includes high-dose systemic steroids. These may diminish optimal antitumor T cell responses, and corticosteroids are not always effective. H11 can partially outcompete full-sized anti–CTLA-4 antibodies for binding to CTLA-4, but the absence of an Fc portion reduces downstream effector function. An anti–CTLA-4 VHH may thus be useful for treatment reversal in patients with life-threatening anti–CTLA-4–induced side effects that are steroid refractory, although this would likely block treatment effects in the tumor microenvironment as well.

Methods

All animals were maintained according to protocols approved by the Massachusetts Institute of Technology (MIT) Committee on Animal Care or the Dana–Farber Cancer Institute (DFCI) Institutional Animal Care and Use Committee. Methods for expression of VHH fusion proteins followed standard procedures as described previously (37). Immunological assays and in vivo tumor experiments followed procedures described elsewhere (37). Details of all experiments are provided in *SI Methods*.

ACKNOWLEDGMENTS. We thank Charles Shoemaker, Jean Mukherjee, and Jacqueline Tremblay (Tufts Cummings Veterinary School) for their assistance with alpaca immunizations; Peter Sage and Arlene Sharpe (Harvard Medical School, Boston, MA) for providing CTLA-4 conditional KO mice; Alica Linnebacher, Christina Martone, Nora Kory, Patti Wisniewski and the Whitehead Flow Cytometry Core (Whitehead Institute for Biomedical Research, Cambridge, MA), and Howard Mak and Scott Malstrom (Koch Institute Animal Imaging and Preclinical Testing, MIT) for technical assistance. Funding was provided by a Ludwig Cancer Research Postdoctoral Fellowship (to J.R.I.); the Claudia Adams Barr Program for Innovative Cancer Research (J.R.I.); De Maag Lever Darm Stichting (O.S.B.); Stichting Bekker-La Bastide-Fonds (O.S.B.); a Cancer Research Institute Postdoctoral Fellowship (to M.R.); the Melanoma Research Alliance (S.K.D.); the Pew Foundation (S.K.D.); National Institutes of Health (NIH) Grants HG008325 (to S.C.A.), GM094662 (to S.C.A.), GM094665 (to S.C.A.), DP1-GM106409-03 (to H.L.P.), and R01-GM100518-04 (to H.L.P.); Albert Einstein Cancer Center Grant P30CA013330 (to S.C.A.); the Lustgarten Foundation (H.L.P.); Mentored Clinical Scientist Development Award 1K08DK114563-01 (to M.D.); NIH Training Grant 1F32CA210568-01 (to M.D.); Center for the Study of Inflammatory Bowel Disease Grant DK043351 (to M.D.); and an American Gastroenterological Association Research Scholars Award (to M.D.).

1. Baumeister SH, Freeman GJ, Dranoff G, Sharpe AH (2016) Coinhibitory pathways in immunotherapy for cancer. *Annu Rev Immunol* 34:539–573.
2. Larkin J, et al. (2015) Combined nivolumab and ipilimumab or monotherapy in untreated melanoma. *N Engl J Med* 373:23–34.
3. Pardoll DM (2012) The blockade of immune checkpoints in cancer immunotherapy. *Nat Rev Cancer* 12:252–264.
4. Hodi FS, et al. (2010) Improved survival with ipilimumab in patients with metastatic melanoma. *N Engl J Med* 363:711–723.
5. Robert C, et al. (2011) Ipilimumab plus dacarbazine for previously untreated metastatic melanoma. *N Engl J Med* 364:2517–2526.
6. Sharma P, Allison JP (2015) The future of immune checkpoint therapy. *Science* 348: 56–61.
7. Gubin MM, et al. (2014) Checkpoint blockade cancer immunotherapy targets tumour-specific mutant antigens. *Nature* 515:577–581.
8. Schumacher TN, Schreiber RD (2015) Neoantigens in cancer immunotherapy. *Science* 348:69–74.
9. Rashidian M, et al. (2015) Noninvasive imaging of immune responses. *Proc Natl Acad Sci USA* 112:6146–6151.
10. Ingram JR, et al. (2017) PD-L1 is an activation-independent marker of brown adipocytes. *Nat Commun* 8:647.
11. Rashidian M, et al. (2017) Predicting the response to CTLA-4 blockade by longitudinal noninvasive monitoring of CD8 T cells. *J Exp Med* 214:2243–2255.
12. Greenwald RJ, Freeman GJ, Sharpe AH (2005) The B7 family revisited. *Annu Rev Immunol* 23:515–548.
13. Sharpe AH, Freeman GJ (2002) The B7-CD28 superfamily. *Nat Rev Immunol* 2:116–126.
14. Linsley PS, et al. (1996) Intracellular trafficking of CTLA-4 and focal localization towards sites of TCR engagement. *Immunity* 4:535–543.
15. Tivol EA, et al. (1995) Loss of CTLA-4 leads to massive lymphoproliferation and fatal multiorgan tissue destruction, revealing a critical negative regulatory role of CTLA-4. *Immunity* 3:541–547.
16. Schubert D, et al. (2014) Autosomal dominant immune dysregulation syndrome in humans with CTLA4 mutations. *Nat Med* 20:1410–1416.
17. Kuehn HS, et al. (2014) Immune dysregulation in human subjects with heterozygous germline mutations in CTLA4. *Science* 345:1623–1627.
18. Zeissig S, et al. (2015) Early-onset Crohn's disease and autoimmunity associated with a variant in CTLA-4. *Gut* 64:1889–1897.
19. Dougan M (2017) Checkpoint blockade toxicity and immune homeostasis in the gastrointestinal tract. *Front Immunol* 8:1547.
20. Wing K, et al. (2008) CTLA-4 control over Foxp3+ regulatory T cell function. *Science* 322:271–275.
21. Paterson AM, et al. (2015) Deletion of CTLA-4 on regulatory T cells during adulthood leads to resistance to autoimmunity. *J Exp Med* 212:1603–1621.
22. van Elsas A, Hurwitz AA, Allison JP (1999) Combination immunotherapy of B16 melanoma using anti-cytotoxic T lymphocyte-associated antigen 4 (CTLA-4) and granulocyte/macrophage colony-stimulating factor (GM-CSF)-producing vaccines induces rejection of subcutaneous and metastatic tumors accompanied by autoimmune depigmentation. *J Exp Med* 190:355–366.
23. Simpson TR, et al. (2013) Fc-dependent depletion of tumor-infiltrating regulatory T cells co-defines the efficacy of anti-CTLA-4 therapy against melanoma. *J Exp Med* 210:1695–1710.
24. Bulliard Y, et al. (2013) Activating Fc γ receptors contribute to the antitumor activities of immunoregulatory receptor-targeting antibodies. *J Exp Med* 210:1685–1693.
25. Selby MJ, et al. (2013) Anti-CTLA-4 antibodies of IgG2a isotype enhance antitumor activity through reduction of intratumoral regulatory T cells. *Cancer Immunol Res* 1: 32–42.
26. Muyldermans S (2013) Nanobodies: Natural single-domain antibodies. *Annu Rev Biochem* 82:775–797.
27. Sockolosky JT, et al. (2016) Durable antitumor responses to CD47 blockade require adaptive immune stimulation. *Proc Natl Acad Sci USA* 113:E2646–E2654.
28. Ramagopal UA, et al. (2017) Structural basis for cancer immunotherapy by the first-in-class checkpoint inhibitor ipilimumab. *Proc Natl Acad Sci USA* 114:E4223–E4232.
29. Voss NR, Gerstein M (2010) 3V: Cavity, channel and cleft volume calculator and extractor. *Nucleic Acids Res* 38:W555–W562.
30. Rashidian M, et al. (2015) Use of 18F-2-fluorodeoxyglucose to label antibody fragments for immuno-positron emission tomography of pancreatic cancer. *ACS Cent Sci* 1:142–147.
31. Dranoff G, et al. (1993) Vaccination with irradiated tumor cells engineered to secrete murine granulocyte-macrophage colony-stimulating factor stimulates potent, specific, and long-lasting anti-tumor immunity. *Proc Natl Acad Sci USA* 90:3539–3543.
32. Higashikawa K, et al. (2014) 64Cu-DOTA-anti-CTLA-4 mAb enabled PET visualization of CTLA-4 on the T-cell infiltrating tumor tissues. *PLoS One* 9:e109866.
33. Dougan M, et al. (2010) IAP inhibitors enhance co-stimulation to promote tumor immunity. *J Exp Med* 207:2195–2206.
34. Jinushi M, et al. (2007) MFG-E8-mediated uptake of apoptotic cells by APCs links the pro- and antiinflammatory activities of GM-CSF. *J Clin Invest* 117:1902–1913.
35. Hodi FS, et al. (2008) Immunologic and clinical effects of antibody blockade of cytotoxic T lymphocyte-associated antigen 4 in previously vaccinated cancer patients. *Proc Natl Acad Sci USA* 105:3005–3010.
36. DiLillo DJ, Ravetch JV (2015) Differential Fc-receptor engagement drives an anti-tumor vaccinal effect. *Cell* 161:1035–1045.
37. Ingram JR, et al. (2017) Localized CD47 blockade enhances immunotherapy for murine melanoma. *Proc Natl Acad Sci USA* 114:10184–10189.
38. Vazquez-Lombardi R, et al. (2017) Potent antitumour activity of interleukin-2-Fc fusion proteins requires Fc-mediated depletion of regulatory T-cells. *Nat Commun* 8: 15373.
39. Arce Vargas F, et al.; Melanoma TRACERx Consortium; Renal TRACERx Consortium; Lung TRACERx Consortium (2017) Fc-optimized anti-CD25 depletes tumor-infiltrating regulatory T cells and synergizes with PD-1 blockade to eradicate established tumors. *Immunity* 46:577–586.
40. Arlauckas SP, et al. (2017) In vivo imaging reveals a tumor-associated macrophage-mediated resistance pathway in anti-PD-1 therapy. *Sci Transl Med* 9:eaal3604.
41. Barnhart BC, Quigley M (2017) Role of Fc-FcγR interactions in the antitumor activity of therapeutic antibodies. *Immunol Cell Biol* 95:340–346.
42. Dougan M, Dranoff G (2009) Immune therapy for cancer. *Annu Rev Immunol* 27: 83–117.
43. Wei SC, et al. (2017) Distinct cellular mechanisms underlie anti-CTLA-4 and anti-PD-1 checkpoint blockade. *Cell* 170:1120–1133.e17.
44. De Groeve K, et al. (2010) Nanobodies as tools for in vivo imaging of specific immune cell types. *J Nucl Med* 51:782–789.
45. Maass DR, Sepulveda J, Pernthaner A, Shoemaker CB (2007) Alpaca (Lama pacos) as a convenient source of recombinant camelid heavy chain antibodies (VHHs). *J Immunol Methods* 324:13–25.
46. Ostrov DA, Shi W, Schwartz JC, Almo SC, Nathenson SG (2000) Structure of murine CTLA-4 and its role in modulating T cell responsiveness. *Science* 290:816–819.